Supporting Information

Hegyi et al. 10.1073/pnas.1718211115

SI Materials and Methods

All animal handling and laboratory procedures followed US National Institutes of Health guidelines and were approved by the Institutional Animal Care and Use Committee of the University of California, Davis.

Animal Model and Cell Isolation. The porcine model of chronic MI used is this study was developed to provide a clinically relevant large-animal ischemic cardiomyopathy model without the frequent adverse complications of the infarct creation (e.g., apical infarcts with frequent inadvertent right ventricular involvement, poor lesion reproducibility, and high perioperative mortality rates reported for models on occlusion of the LAD coronary artery) and where the lesion location is amenable to noninvasive echocardiographic imaging allowing for longitudinal monitoring of post-MI LV dysfunction (1). Yucatan minipigs were obtained from S&S Farms and acclimated for at least 10 d before surgery happened.

In 12 adult Yucatan minipigs (4–6 mo-old, 45–60 kg) transmural MI was induced by targeted microbead embolization of the first diagonal branch of the LAD coronary artery via injection of 2-mL 90-μm diameter polystyrene microspheres (Polybead, Polysciences), resulting in significant LV dysfunction and remodeling (1). Progression of cardiac structural and functional remodeling was monitored immediately postoperatively, 8-wk post-MI, and at the 5-mo endpoint by using 2D and M-mode echocardiography (Table S1). LV EF decreased from the preoperative 69.85 ± 2.32% to 47.13 ± 5.64% at the 5-mo endpoint when the ventricular cells were isolated. These pigs were part of a larger study examining the proregenerative mechanism and outcome of mesenchymal stem cells seeded extracellular matrix scaffolds (2). For the HF group, we used pigs that underwent sham or matrix patch implantation (no cells) 8 wk post-MI. As control group, we used tissue from healthy age-matched minipigs that were implanted with a patch on their RV after a 2-cm resection of the wall (these animals were also administered BrDU). At the end of the follow-up period, the pigs were killed under general inhalation anesthesia. Following thoracotomy, the heart was placed in a cardioplegic solution in situ before excision (solution contained: $CaCl_2$ 1.2 mmol/L, $MgCl_2$ 34.1 mmol/L, KCl 16 mmol/L, $NaHCO_3$ 10 mmol/L, and NaCl 110 mmol/L). This was followed by perfusion with custodial HTK solution (containing: NaCl 15 mmol/L, KCl 9 mmol/L, $MgCl_2$ 4 mmol/L, L-histidine hydrochloride 18 mmol/L, L-histidine 180 mmol/L, tryptophan 2 mmol/L, mannitol 30 mmol/L, $CaCl_2$ 0.015 mmol/L, and potassium hydrogen 2-ketoglutarate 2 mmol/L) supplemented with 10 mmol/L 2,3-butanedione monoxime. For functional cell studies, LV cardiomyocytes from the remote or border zone of the infarct were obtained by enzymatic digestion using cannulation and perfusion of the left coronary vasculature (either coronary sinus or the left circumflex coronary artery) or a chunk method. The respective procedures were performed as described previously using 1.6 mg/mL collagenase B (Roche Diagnostics) and 0.025 mg/mL protease (Sigma-Aldrich) (3, 4).

Reagents. Chemicals and reagents were purchased from Sigma-Aldrich, if not specified otherwise. E-4031 and HMR-1556 were from Tocris Bioscience. ORM-10962 was from Orion Pharma. GS-458967 was from Gilead Sciences.

Electrophysiology. APs and underlying ionic currents were recorded using whole-cell patch-clamp under physiological conditions with preserved Ca^{2+} cycling (cell having physiological $[Ca^{2+}_i]$ transient and contraction) during AP. Isolated cells were transferred to a temperature controlled Plexiglas chamber (Cell Microsystems) and continuously superfused with a bicarbonate containing oxygenized Tyrode (BTY) solution containing: NaCl 124 mmol/L, $NaHCO_3$ 25 mmol/L, KCl 4 mmol/L, $CaCl_2$ 1.2 mmol/L, $MgCl_2$ 1 mmol/L, Hepes 10 mmol/L, glucose 10 mmol/L, with pH 7.4. Electrodes were fabricated from borosilicate glass (World Precision Instruments) with tip resistances of 2–2.5 MΩ when filled with internal solution containing: K-Aspartate 110 mmol/L, KCl 25 mmol/L, NaCl 5 mmol/L, Mg-ATP 3 mmol/L, Hepes 10 mmol/L, cAMP 0.002 mmol/L, phosphocreatine-K_2 salt 10 mmol/L, EGTA 0.01 mmol/L, with pH 7.25. This composition preserved the physiological Ca^{2+} cycling (5, 6). The osmolality of all applied solutions was carefully adjusted to 298 ± 3 mOsm with a vapor pressure osmometer (Vapro 5520; Wescor). The electrodes were connected to the input of an Axopatch 200B amplifier (Axon Instruments). Outputs from the amplifier were digitized at 50 kHz using a Digidata 1440A A/D converter (Molecular Devices) under software control (pClamp 10; Molecular Devices). The series resistance was typically 3–5 MΩ and it was compensated by 90%. Experiments were discarded if the series resistance was higher or increased by more than 10% during the measurement. Reported AP voltages are already corrected for the liquid junction potential. All electrophysiological experiments were conducted at 36 ± 0.1 °C.

APs were recorded in I-clamp experiments where cells were stimulated with suprathreshold depolarizing pulses (2-ms duration) delivered via the patch pipette. Following 3 min of adaptation at a given frequency (from 0.2 Hz to 5 Hz), 50 consecutive APs were recorded and analyzed. APD at 95% of repolarization (APD_{95}) was used to assess precisely the influence of NCX function, which is known to be altered in HF (3), on AP profile when measured under physiological conditions (5). Series of 50 consecutive APs were analyzed to estimate STV of AP duration according to the following formula: $STV = \Sigma\,(\,|\,APD_{i+1} - APD_i\,|\,)/[(n_{beats} - 1) \times \sqrt{2}]$, where APD_n and APD_{n+1} indicate the durations of the i^{th} and $(i + 1)^{th}$ APs, and n_{beats} denotes the number of consecutive beats analyzed (7, 8). Changes in STV are presented as Poincaré plots, where 50 consecutive APD_{95} values are plotted, each against the duration of the previous AP (Fig. S2). To analyze further the variability of repolarization, the difference between consecutive APD_{95} values were grouped in millisecond ranges and the overall probability of their appearance was calculated in each cell. Then the average of these data were plotted to illustrate the changes in beat-to-beat variability of APD (9).

Diastolic arrhythmogenic activities were elicited by cessation of 3 min of burst pacing (5 Hz), and membrane potential were recorded for additional 3 min. DADs were defined as an increase in resting membrane potential exceeding 1.5 mV in amplitude within 0.5 s. tAPs were defined as depolarizations initiated by a DAD then having a fast upstroke phase (exceeding 0 mV). The term of complex tAP was used when an EAD superimposed on the tAP. EAD was defined as the inflection of membrane potential change during repolarization, exceeding 3 mV in amplitude. DAD parameters were assessed only in those events where no tAP occurred subsequently. DAD amplitude data were fitted to a log-normal distribution curve. Pharmacological modulation of DAD parameters was performed by preincubating the cells with different drugs (dissolved in Tyrode) for 10 min before starting the experiment. The role of $I_{Cl(Ca)}$, I_{NCX}, and I_{NaL} in DAD generation was investigated by their selective inhibitors, 9-anthracenecarboxylic

acid (0.5 mmol/L), ORM-10962 (500 nmol/L), and GS-458967 (1 μmol/L), respectively. CaMKII inhibition was achieved by using KN-93 (3 μmol/L).

The ^{self}AP-clamp sequential dissection experiments were conducted as previously described (5, 6, 9–12). Briefly, the basic steps are as follows: (Step 1) Record the cell's steady-state AP under I-clamp ($I = 0$) at chosen pacing frequency. (Step 2) Apply this AP onto the same cell as the voltage command under V-clamp at the same pacing frequency. The net current output ($I_{Reference}$) after reaching steady-state should be zero. (Step 3) Isolate the current of interest by using its specific blocker to remove it from the net current output, I_{Drug}. (Step 4) The current of interest is obtained by subtraction: $I_{Difference} = I_{Reference} - I_{Drug}$. (Step 5) Next, isolate the second current of interest (I_2) by applying the second channel blocker, and then obtain the second current by subtraction: $I_2 = I_{Drug1} - I_{Drug2}$. Repeat step 5 to isolate the third, the fourth, and more currents by sequentially adding the specific blocker for each ion channel in a cumulative manner and obtain the difference current. Note that all currents were recorded after their specific blocker had reached steady-state effect. Using local perfusion, steady-state effect was achieved within 2 min in all cases. Ionic currents were dissected by specific inhibitors used in a sequence minimizing the adverse effects of a blocker on other ion channels (e.g., nifedipine), blocker of I_{CaL} was used only as a last step to preserve Ca^{2+} cycling and its influence on other ionic currents (via CaM, CaMKII, and other Ca^{2+}-dependent signaling pathways). The following sequence of selective blockers was used for dissecting out the specific currents: 1 μmol/L GS-458967 for I_{NaL}, 100 nmol/L apamin for $I_{K(Ca)}$, 1 μmol/L HMR-1556 for I_{Ks}, 1 μmol/L E-4031 for I_{Kr}, 0.5 mmol/L 9-anthracenecarboxylic acid for $I_{Cl(Ca)}$, 100 μmol/L $BaCl_2$ for I_{K1}, 0.5 μmol/L ORM-10962 for I_{NCX}, 10 μmol/L nifedipine for I_{CaL} (see also Table S2 for drug-selectivity data). This method enables us to examine how the AP is shaped by the counterbalancing act of the inward currents and the outward currents in the same cell, allowing fingerprinting of the individual cell electrophysiology (shown in Fig. S1).

Conventional voltage-clamp measurement of I_{K1} was conducted in the presence of 10 mmol/L EGTA in the pipette solution (without adding any Ca^{2+}) and the Tyrode solution was supplemented with 10 μmol/L tetrodotoxin, 10 μmol/L nifedipine, 1 μmol/L HMR-1556 and 1 μmol/L E-4031 to block I_{Na}, I_{CaL}, I_{Ks}, and I_{Kr}, respectively. Then, experiments were repeated following the perfusion of 100 μmol/L $BaCl_2$ to inhibit I_{K1}. Steady-state current–voltage relationships were obtained by plotting the magnitude of the Ba^{2+}-sensitive current traces recorded at the end of 500-ms test pulse as a function of the test depolarization, arising from the holding potential of −80 mV (Fig. S3).

Ionic currents were normalized to cell capacitance, determined in each cell using short (10 ms) hyperpolarizing pulses from −10 to −20 mV. Cell capacitance was 138.26 ± 4.26 pF in control (n = 23 cells/5 animals), 172.24 ± 6.50 pF in HF-Remote (n = 29 cells/7 animals), and 170.94 ± 5.20 pF in the HF-border (n = 35 cells/7 animals), respectively.

To characterize each ionic current, we report the current density (current magnitude/cell capacitance) and the net charge carried by the given ionic current during the AP (from AP peak to APD_{95}).

Simultaneous Measurement of Cardiomyocyte Contraction and Intracellular Ca^{2+} Transient. To measure cardiomyocyte contraction the IonOptix sarcomere detection and fast Fourier transform (FFT) method was used. Contraction was measured using an IonOptix system (IonOptix Co.) with a high-speed camera (MyoCam-S, 240–1,000 frames/s) to record sarcomere movement during cardiomyocyte contraction. The sarcomere pattern was then used to calculate the sarcomere length using an FFT algorithm. The fractional shortening was then calculated as the percentage of change in sarcomere length during contraction.

To measure the intracellular Ca^{2+} concentration, a Fura-2 dual-wavelength ratiometric method was used (13). Freshly isolated cardiomyocytes were loaded in Tyrode solution with the membrane-permeant form of Fura-2 (Fura-2AM, 5 μmol/L) in the presence of Pluronic F127 (0.75 μmol/L in 20% dimethyl sulfoxide) for 30 min at room temperature, then washed, and used for experiments within 8 h. Cells were placed in a measuring chamber and continuously superfused at room temperature (22 ± 1 °C) or at body temperature (36 ± 0.1 °C) with an oxygenized modified Tyrode solution containing: NaCl 120 mmol/L, $NaHCO_3$ 25 mmol/L, KCl 4 mmol/L, $CaCl_2$ 1 mmol/L, $MgCl_2$ 1 mmol/L, Hepes 10 mmol/L, Pyruvic acid 5 mmol/L, Taurine 15 mmol/L, with pH 7.4. During measurements cells were continuously paced at 0.5-Hz frequency by electrical field stimulation using short (4 ms) depolarization pulses with bipolar switching (switch positive and negative polarity in consecutive stimulus pulses) applied with a pair of platinum electrodes. An IonOptix system with a HyperSwitch was mounted on the Olympus 71× inverted microscope with a water immersion fluorescence objective UPlanSApo 40×, 1.15 numerical aperture (NA) (corrected for the thickness of the no. 1 glass coverslip used as the bottom of the chamber). The excitation light was generated using a high-intensity arc lamp (Cairn Research). The galvanometer-based HyperSwitch delivered dual-excitation beams at 340 and 380 nm using a 340/370d/380 filter cube, switching between the two wavelengths at a frequency of 500 Hz. Fura-2 fluorescence emission light was passed through a bandpass filter D510/40m and collected by a photon multiplier tube (PMT). The Fura-2 fluorescence ratio, F_{340}/F_{380}, was calculated from the fluorescence emissions from cells at 340- and 380-nm excitation wavelengths after background subtraction. For measuring systolic Ca^{2+} transient, the cell was first paced to reach steady state (>3 min), and then Fura-2 fluorescence was recorded for at least 10 consecutive beats during steady-state.

Confocal Imaging of Ca^{2+} Signals. Elementary Ca^{2+} release events (Ca^{2+} sparks) in intact cardiomyocytes were detected with confocal imaging of Fluo-4 signals (13). Freshly isolated cardiomyocytes were loaded in Tyrode solution with the membrane permeant form of Fluo-4 (Fluo-4AM, 2.5 μmol/L) in the presence of Pluronic F127 (0.75 μmol/L in 20% dimethyl sulfoxide) for 20 min at room temperature, then washed for 15 min, and used for experiments within 6 h. Cells were placed in a measuring chamber and continuously superfused at room temperature (22 ± 1 °C) with an oxygenized modified Tyrode solution containing: NaCl 120 mmol/L, $NaHCO_3$ 25 mmol/L, KCl 4 mmol/L, $CaCl_2$ 1 mmol/L, $MgCl_2$ 1 mmol/L, Hepes 10 mmol/L, Pyruvic acid 5 mmol/L, Taurine 15 mmol/L, with pH 7.4. Spontaneous Ca^{2+} sparks were recorded following cessation of 3 min of field stimulation at 0.5-Hz frequency (4-ms depolarization pulses with bipolar switching).

Confocal imaging was performed with an Olympus FluoView FV1000 laser scanning confocal microscope (inverted configuration) with a water immersion fluorescence objective UPlanSApo 60×, 1.2 NA (corrected for the thickness of the no. 1 glass coverslip that is used as the bottom of the chamber). Fluo-4 was excited with a 488-nm laser beam (laser power was set to 5%), then the emitted fluorescence light passed through a bandpass filter BA505-605 and were collected by a PMT. The PMT voltage, gain, and offset were set to avoid saturation and to obtain high-fidelity images. Linescan images were obtained using the highest scan speed of 2 μs per pixel. Ca^{2+} sparks were detected automatically by a custom-made program based on our spark identification algorithm and adapted for x-t linescan images as previously described (13, 14). Sparks were identified in two steps. First, putative sparks were detected based on Cheng et al.'s (15) description, and bright but spatially small events were eliminated

using our previously described "live-or-die" algorithm (16). Second, the putative sparks were classified as sparks or noise based on the statistical sieve as previously described (14). This analysis software provides automated and objective (agnostic through statistical sieving) detection and classification of the elementary Ca^{2+} release events in confocal linescan images.

Echocardiography. All echocardiographic assessment was done with a S5-1 linear probe (iE33 xMatrix ultrasound; Philips Healthcare). Animals were in dorsal recumbency during imaging under anesthesia (during MI induction) or deep sedation (during follow-up at 8 wk and 5 mo post-MI). Standard LV outflow tract view performed from the right parasternal location was used for both 2D and M-mode assessments (1). Three consecutive cardiac cycles were measured and averaged for each animal.

Data Availability. All relevant data have been deposited and are publicly available at https://doi.org/10.25338/B88593.

1. Hanes DW, et al. (2015) Embolization of the first diagonal branch of the left anterior descending coronary artery as a porcine model of chronic trans-mural myocardial infarction. *J Transl Med* 13:187.
2. Papalamprou A, Griffiths LG (2016) Cardiac extracellular matrix scaffold generated using sarcomeric disassembly and antigen removal. *Ann Biomed Eng* 44:1047–1060.
3. Fischer TH, et al. (2013) Ca2+/calmodulin-dependent protein kinase II and protein kinase A differentially regulate sarcoplasmic reticulum Ca2+ leak in human cardiac pathology. *Circulation* 128:970–981.
4. Nichols CB, et al. (2014) β-adrenergic signaling inhibits Gq-dependent protein kinase D activation by preventing protein kinase D translocation. *Circ Res* 114:1398–1409.
5. Banyasz T, Horvath B, Jian Z, Izu LT, Chen-Izu Y (2012) Profile of L-type Ca(2+) current and Na(+)/Ca(2+) exchange current during cardiac action potential in ventricular myocytes. *Heart Rhythm* 9:134–142.
6. Horvath B, et al. (2013) Dynamics of the late Na(+) current during cardiac action potential and its contribution to afterdepolarizations. *J Mol Cell Cardiol* 64:59–68.
7. Johnson DM, et al. (2013) Diastolic spontaneous calcium release from the sarcoplasmic reticulum increases beat-to-beat variability of repolarization in canine ventricular myocytes after β-adrenergic stimulation. *Circ Res* 112:246–256.
8. Szentandrássy N, et al. (2015) Contribution of ion currents to beat-to-beat variability of action potential duration in canine ventricular myocytes. *Pflugers Arch* 467: 1431–1443.
9. Hegyi B, et al. (2017) Ca^{2+}-activated Cl^-current is antiarrhythmic by reducing both spatial and temporal heterogeneity of cardiac repolarization. *J Mol Cell Cardiol* 109: 27–37.
10. Banyasz T, Horvath B, Jian Z, Izu LT, Chen-Izu Y (2011) Sequential dissection of multiple ionic currents in single cardiac myocytes under action potential-clamp. *J Mol Cell Cardiol* 50:578–581.
11. Chen-Izu Y, Izu LT, Hegyi B, Bányász T (2017) Recording of ionic currents under physiological conditions: Action potential-clamp and 'Onion-Peeling' techniques. *Modern Tools of Biophysics*, ed Jue T (Springer, New York), pp 31–48.
12. Horváth B, et al. (2016) Sarcolemmal Ca(2+)-entry through L-type Ca(2+) channels controls the profile of Ca(2+)-activated Cl(-) current in canine ventricular myocytes. *J Mol Cell Cardiol* 97:125–139.
13. Jian Z, et al. (2014) Mechanochemotransduction during cardiomyocyte contraction is mediated by localized nitric oxide signaling. *Sci Signal* 7:ra27.
14. Bányász T, Chen-Izu Y, Balke CW, Izu LT (2007) A new approach to the detection and statistical classification of Ca2+ sparks. *Biophys J* 92:4458–4465.
15. Cheng H, et al. (1999) Amplitude distribution of calcium sparks in confocal images: Theory and studies with an automatic detection method. *Biophys J* 76:606–617.
16. Chen-Izu Y, et al. (2006) Three-dimensional distribution of ryanodine receptor clusters in cardiac myocytes. *Biophys J* 91:1–13.

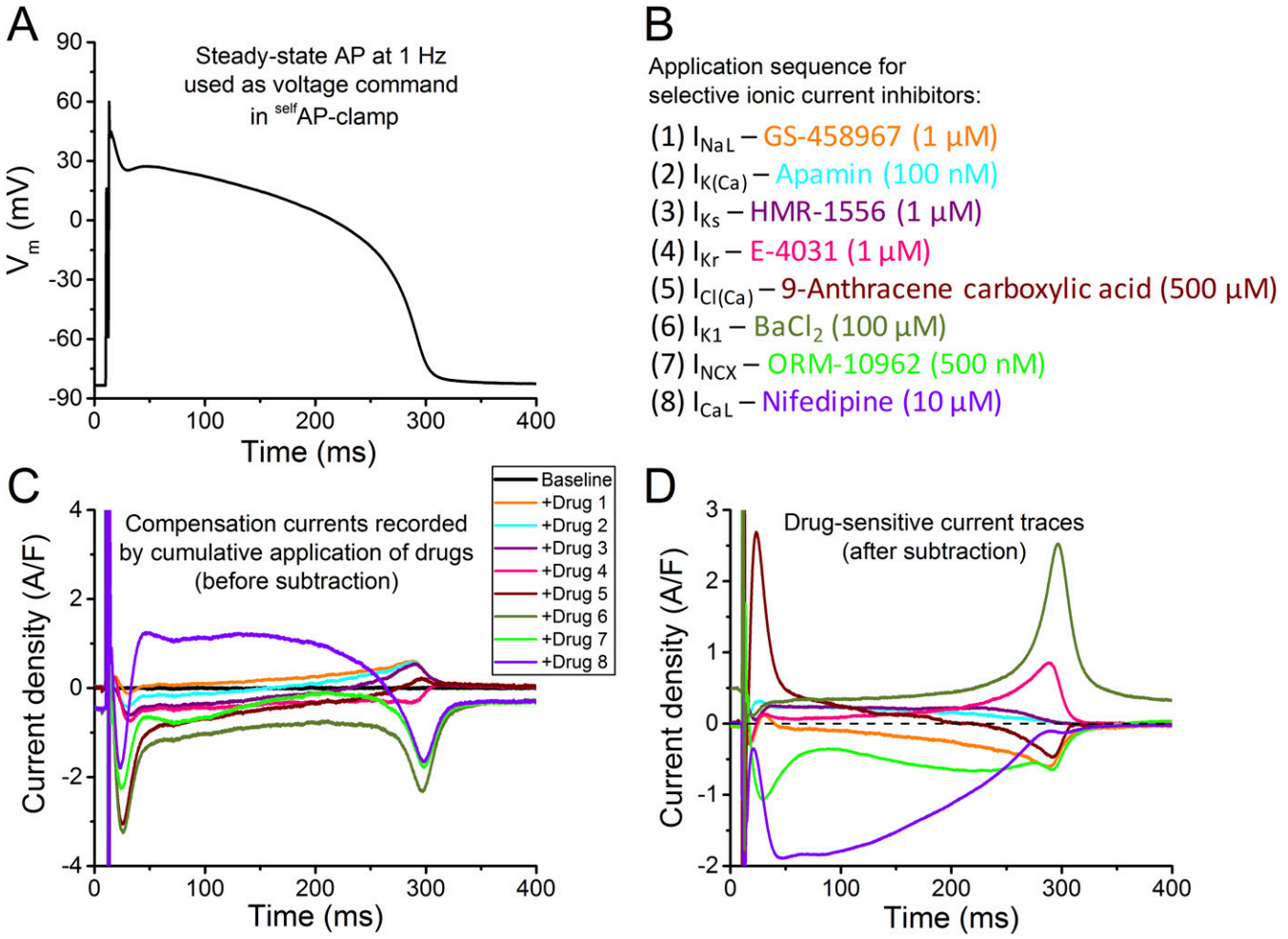

Fig. S1. Sequential dissection of ionic currents with selfAP-clamp technique. By using selfAP-clamp technique multiple current can be measured on the same cell under physiological conditions (under the cell's own steady-state AP measured with preserved Ca^{2+} cycling and cell contraction until the application of nifedipine in the last step, which abolished cell contraction as it was expected) representing a prominent tool toward individual cell electrophysiology. (*A*) Representative AP recorded in current-clamp at 1-Hz steady-state pacing frequency in a pig ventricular myocyte. (*B*) Applied sequence and concentration of the selective blockers of ion channels/transporters (see also Table S2). (*C*) Representative compensation current traces during the applied protocol in selfAP-clamp sequential dissection experiments. Baseline current obtained under these conditions is a horizontal line positioned at the zero level except for the very short segment corresponding to the AP upstroke and capacitive transient. The drugs listed in *B* were applied in a cumulative manner and the compensation currents were recorded after each drug reached its steady-state effect. (*D*) Representative drug-sensitive current traces after subtracting the drug-induced compensation current traces from their corresponding reference current traces measured before the application of each drug (for more details, see *Electrophysiology* section of *SI Materials and Methods*).

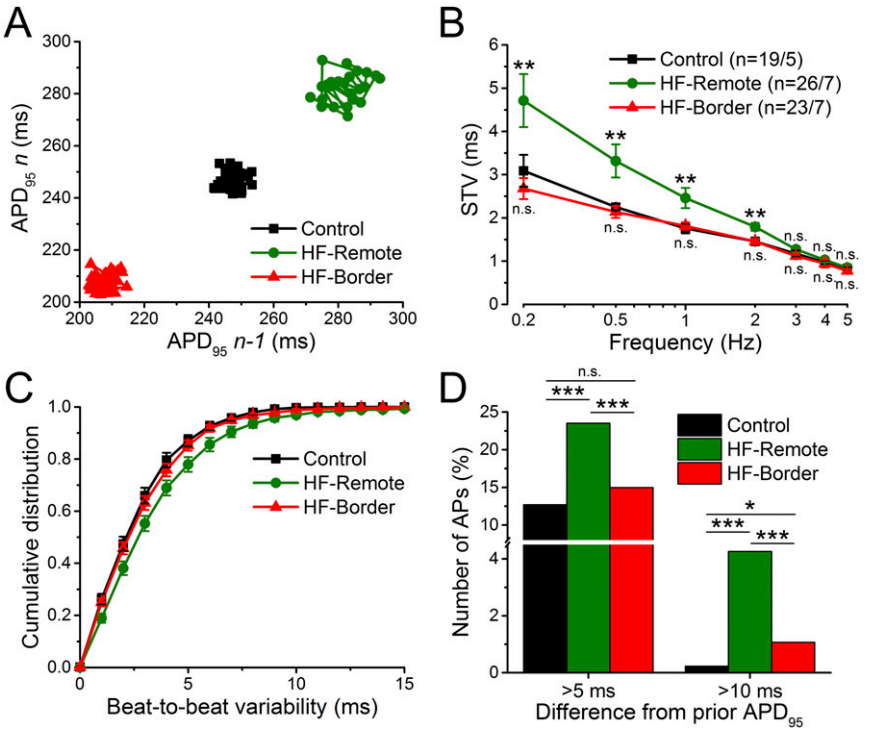

Fig. S2. Increased temporal variability of APD in ischemic HF. (*A*) Representative Poincare plots of 50 consecutive APD_{95} values in control, HF-remote, and HF-border cells at 1-Hz steady-state pacing. (*B*) Frequency-dependent STV of APD_{95}. (*C*) Cumulative distribution curves of individual beat-to-beat variability values at 1-Hz pacing. (*D*) Percentage of total APs measured at 1-Hz pacing having beat-to-beat APD_{95} variability of >5 ms and >10 ms in consecutive beats. Mean ± SEM, n = 19–26 cells/5–7 animals. ANOVA with Bonferroni posttest; n.s., not significant, $*P < 0.05$, $**P < 0.01$, $***P < 0.001$.

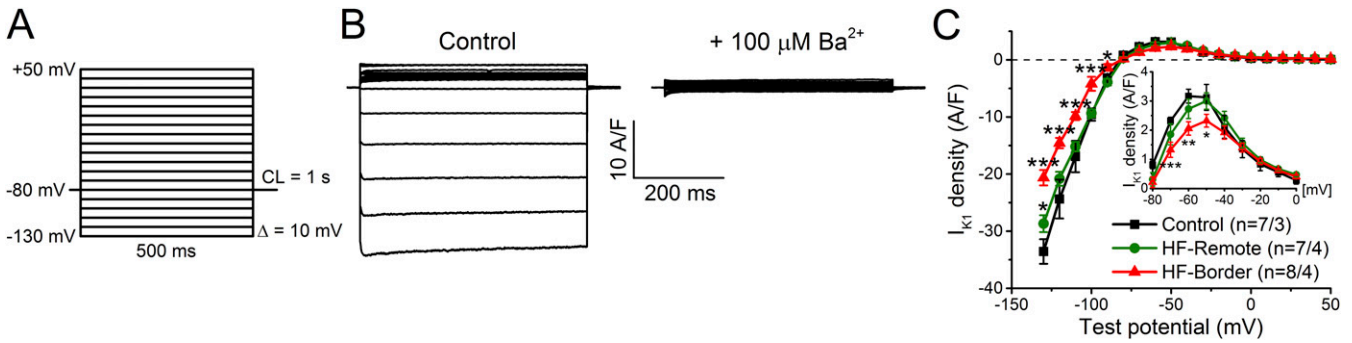

Fig. S3. Decreased I_{K1} density in the border zone of the infarcted pig heart. (*A*) Voltage-clamp protocol used to elicit inward rectifier K^+ current (I_{K1}). (*B*) Representative I_{K1} current traces before and after perfusion with 100 μmol/L Ba^{2+} in control. I_{K1} was defined as Ba^{2+}-sensitive current. (*C*) Current–voltage (I–V) relationships of I_{K1} in control, HF-remote, and HF-border cells. Outward I_{K1} I–V is enlarged (*Inset*). Mean ± SEM, n = 7–8 cells/3–4 animals. ANOVA with Bonferroni posttest; $*P < 0.05$, $**P < 0.01$, $***P < 0.001$ vs. control.

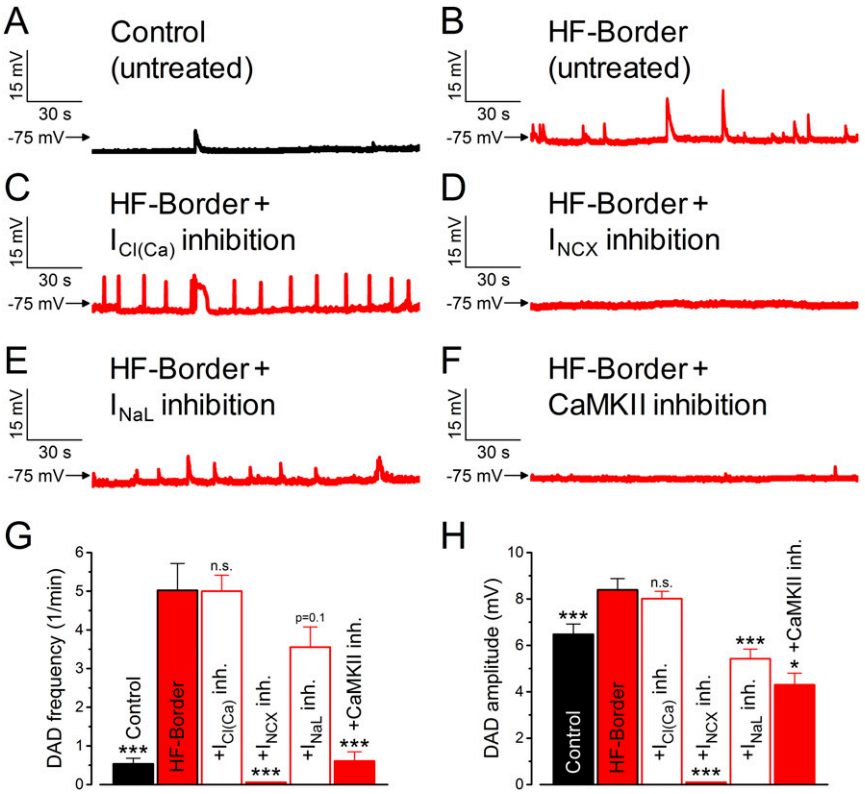

Fig. S4. Pharmacological modulation of delayed afterdepolarizations in ischemic HF. DADs were elicited by cessation of burst pacing (3 min at 5 Hz). (*A*) Representative recording of the membrane potential in a control myocyte exhibiting two DADs with small amplitude during 3-min resting period (total n = 18 cells/5 animals in control). (*B*) Representative record of a HF-border cell having several DADs with larger amplitude (total n = 27 cells/7 animals in untreated HF-border). (*C*) Inhibition of the Ca^{2+}-activated Cl^- current [$I_{Cl(Ca)}$] by 0.5 mmol/L 9-anthracenecarboxylic acid had no effect on the frequency and the amplitude of DADs in the HF-border (total n = 6 cells/4 animals). (*D*) Inhibition Na^+/Ca^{2+} exchange current (I_{NCX}) by 500 nmol/L ORM-10962 abolished DADs in the HF-border (total n = 6 cells/3 animals). (*E*) Inhibition of late Na^+ current (I_{NaL}) by 1 μmol/L GS-458967 decreased the amplitude of DADs in the HF-border (total n = 6 cells/4 animals). (*F*) Inhibition of the Ca^{2+}-CaMKII by 3 μmol/L KN-93 significantly reduced both the frequency and the amplitude of DADs in the HF-border (total n = 6 cells/3 animals). (*G*) Statistics on DAD frequency. (*H*) Statistics on DAD amplitude. DAD was defined as more than 1.5-mV depolarization of the resting membrane potential. Cells were preincubated for 10 min with the given drug before the recording started. Control values are shown for comparison. Mean ± SEM. ANOVA with Bonferroni posttest; n.s., not significant, $*P < 0.05$, $**P < 0.01$, $***P < 0.001$ vs. untreated HF-border.

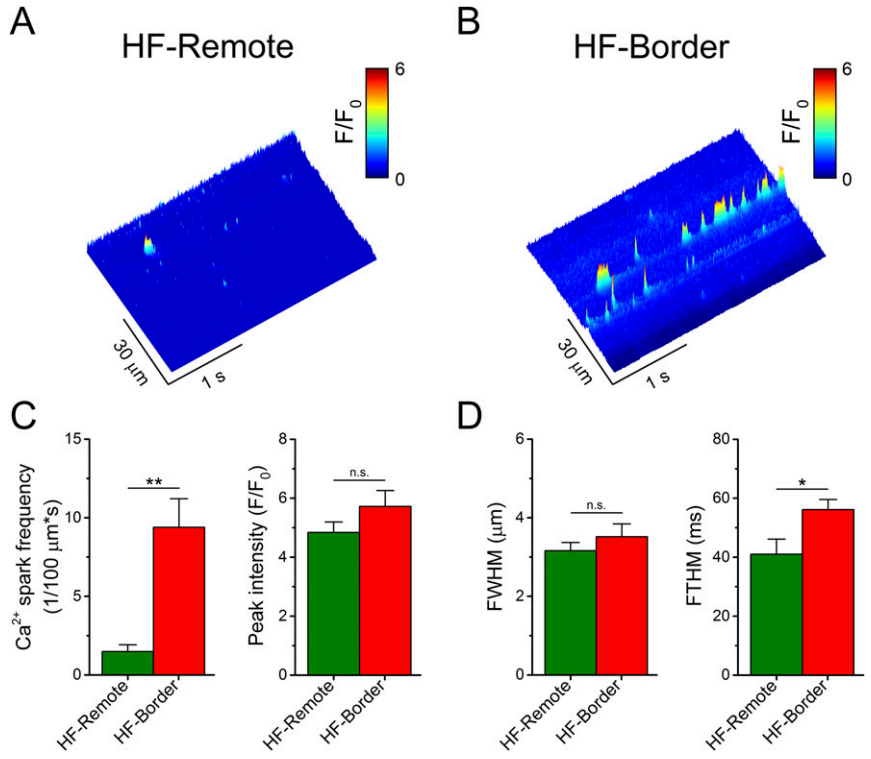

Fig. S5. Confocal imaging of Ca^{2+} signals in ischemic HF. (*A* and *B*) Spontaneous Ca^{2+} sparks shown in the 3D display of confocal linescan images of Fluo-4 signals obtained in representative HF-remote (*Left*) and HF-border (*Right*) cells. (*C*) Ca^{2+} spark frequency was markedly increased in HF-border compared with HF-remote with similar fluorescence intensity in both regions. (*D*) Spatial width (full-width at half-maximum, FWHM) was not different between the HF-remote and HF-border; however, the duration (full-time at half-maximum, FTHM) was significantly increased in the HF-border. Mean ± SEM, n = 5–7 cells/2 animals. ANOVA with Bonferroni posttest; n.s., not significant, $*P < 0.05$, $**P < 0.01$.

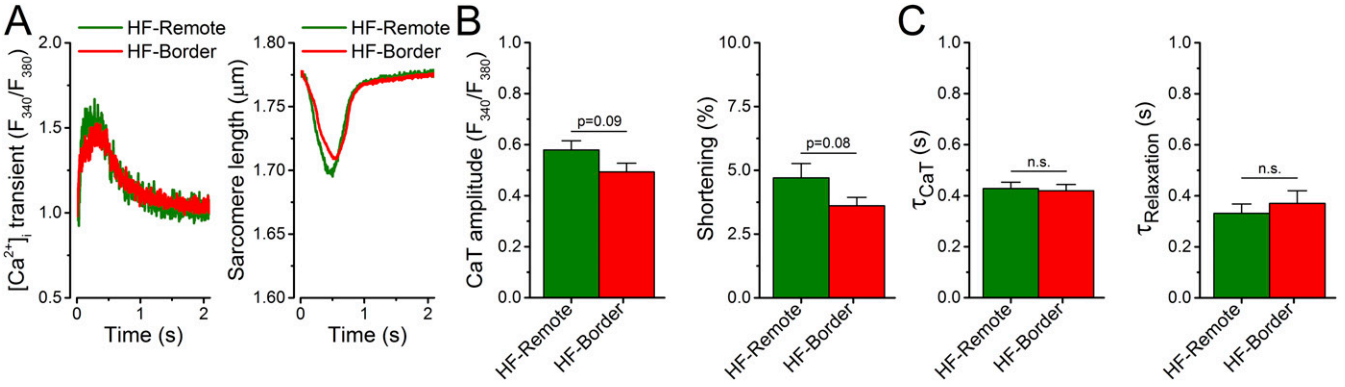

Fig. S6. Comparison of $[Ca^{2+}]_i$ transient and contraction between HF-remote and HF-border at physiological temperature. (*A*) Representative $[Ca^{2+}]_i$ transient and simultaneously recorded sarcomere shortening at body temperature (36 °C) evoked by field stimulation at 0.5-Hz pacing frequency. (*B*) No significant difference was found in $[Ca^{2+}]_i$ transient amplitude and sarcomere shortening between the two HF zones. (*C*) The time constants (τ) of $[Ca^{2+}]_i$ decline and relaxation were accelerated significantly with warming (compare results with that obtained at room temperature in Fig. 2); however, no difference was observed between the HF-remote and HF-border. Mean ± SEM, n = 17 cells/4 animals and 27 cells/4 animals in the HF-remote and HF-border, respectively. ANOVA with Bonferroni posttest; n.s., not significant.

Table S1. LV parameters assessed by echocardiography

Ventricular parameter	Pre-MI	Ischemic HF
EF, %	69.85 ± 2.32	45.23 ± 5.89***
EDV, mL	64.73 ± 4.40	91.28 ± 5.30***
ESV, mL	19.57 ± 2.03	42.27 ± 7.53**
IDd, mm	38.46 ± 1.16	43.58 ± 1.69*
IDs, mm	23.37 ± 1.03	30.10 ± 3.28$^{P = 0.055}$
IVSd, mm	8.85 ± 0.31	9.58 ± 0.62$^{n.s.}$
IVSs, mm	14.25 ± 0.53	12.58 ± 0.78$^{n.s.}$
PWd, mm	7.62 ± 0.24	9.11 ± 0.72$^{P = 0.054}$
PWs, mm	15.58 ± 0.45	13.18 ± 1.11$^{P = 0.052}$

LV dimensions measured in M-mode echocardiography prior MI induction and at the 5-mo endpoint demonstrate ventricular dilation and functional impairment. All data represent mean ± SEM $n = 12$ animals. Student's two-tailed paired t test; n.s., not significant, *$P < 0.05$, **$P < 0.01$, ***$P < 0.001$. EF, ejection fraction calculated as EF = (EDV−ESV)/EDV × 100); EDV, end diastolic volume; ESV, end systolic volume; IDd, internal diameter at end diastole; IDs, internal diameter at end systole; IVSd, interventricular septal thickness at end diastole; IVSs, interventricular septal thickness at end systole; PWd, posterior wall thickness at end diastole; PWs, posterior wall at end systole.

Table S2. Blockers used to measure specific drug-sensitive ionic currents in ^{self}AP-clamp

Current	Blocker	Dose, μmol/L	Refs.
Late Na^+ current (I_{NaL})	GS-458967	1	(1, 2)
Ca^{2+}-activated K^+ current [$I_{K(Ca)}$]	Apamin	100	(3, 4)
Slow delayed rectifier K^+ current (I_{Ks})	HMR-1556	1	(5, 6)
Rapid delayed rectifier K^+ current (I_{Kr})	E-4031	1	(7, 8)
Inward rectifier K^+ current (I_{K1})	Ba^{2+}	100	(9, 10)
Ca^{2+}-activated Cl^- current [$I_{Cl(Ca)}$]	9-Anthracenecarboxylic acid	500	(11, 12)
Na^+/Ca^{2+} exchanger current (I_{NCX})	ORM-10962	500	(13, 14)
L-type Ca^{2+} current (I_{CaL})	Nifedipine	10	(15, 16)

List of drugs in the order of application in ^{self}AP-clamp experiments. These drugs are potent and selective inhibitors of individual ionic currents in the applied dosage. For more details, see the references cited within the table.

1. Belardinelli L, et al. (2013) A novel, potent, and selective inhibitor of cardiac late sodium current suppresses experimental arrhythmias. *J Pharmacol Exp Ther* 344:23–32.
2. Koltun DO, et al. (2016) Discovery of triazolopyridine GS-458967, a late sodium current inhibitor (Late INai) of the cardiac NaV 1.5 channel with improved efficacy and potency relative to ranolazine. *Bioorg Med Chem Lett* 26:3202–3206.
3. Adelman JP, Maylie J, Sah P (2012) Small-conductance Ca2+-activated K+ channels: Form and function. *Annu Rev Physiol* 74:245–269.
4. Yu CC, Ai T, Weiss JN, Chen PS (2014) Apamin does not inhibit human cardiac Na+ current, L-type Ca2+ current or other major K+ currents. *PLoS One* 9:e96691.
5. Gerlach U, et al. (2001) Synthesis and activity of novel and selective I(Ks)-channel blockers. *J Med Chem* 44:3831–3837.
6. Thomas GP, Gerlach U, Antzelevitch C (2003) HMR 1556, a potent and selective blocker of slowly activating delayed rectifier potassium current. *J Cardiovasc Pharmacol* 41:140–147.
7. Wettwer E, Scholtysik G, Schaad A, Himmel H, Ravens U (1991) Effects of the new class III antiarrhythmic drug E-4031 on myocardial contractility and electrophysiological parameters. *J Cardiovasc Pharmacol* 17:480–487.
8. Liu DW, Antzelevitch C (1995) Characteristics of the delayed rectifier current (IKr and IKs) in canine ventricular epicardial, midmyocardial, and endocardial myocytes. A weaker IKs contributes to the longer action potential of the M cell. *Circ Res* 76:351–365.
9. Alagem N, Dvir M, Reuveny E (2001) Mechanism of Ba(2+) block of a mouse inwardly rectifying K+ channel: Differential contribution by two discrete residues. *J Physiol* 534:381–393.
10. Zaza A, Rocchetti M, Brioschi A, Cantadori A, Ferroni A (1998) Dynamic Ca2+-induced inward rectification of K+ current during the ventricular action potential. *Circ Res* 82:947–956.
11. Li GR, Sun H, To J, Tse HF, Lau CP (2004) Demonstration of calcium-activated transient outward chloride current and delayed rectifier potassium currents in swine atrial myocytes. *J Mol Cell Cardiol* 36:495–504.
12. Váczi K, et al. (2015) 9-Anthracene carboxylic acid is more suitable than DIDS for characterization of calcium-activated chloride current during canine ventricular action potential. *Naunyn Schmiedebergs Arch Pharmacol* 388:87–100.
13. Kohajda Z, et al. (2016) The effect of a novel highly selective inhibitor of the sodium/calcium exchanger (NCX) on cardiac arrhythmias in in vitro and in vivo experiments. *PLoS One* 11: e0166041.
14. Oravecz K, et al. (2018) Inotropic effect of NCX inhibition depends on the relative activity of the reverse NCX assessed by a novel inhibitor ORM-10962 on canine ventricular myocytes. *Eur J Pharmacol* 818:278–286.
15. Charnet P, Ouadid H, Richard S, Nargeot J (1987) Electrophysiological analysis of the action of nifedipine and nicardipine on myocardial fibers. *Fundam Clin Pharmacol* 1:413–431.
16. Shen JB, Jiang B, Pappano AJ (2000) Comparison of L-type calcium channel blockade by nifedipine and/or cadmium in guinea pig ventricular myocytes. *J Pharmacol Exp Ther* 294:562–570.